

STRUCTURAL ANALYSIS CASE STUDIES OF BUILDINGS DAMAGED DURING THE TOHOKU TSUNAMI

Lyle Carden¹, Gary Chock¹, Ian Robertson² and Guangren Yu¹

¹Martin & Chock, Inc.

²University of Hawaii at Manoa
Honolulu, Hawaii/USA

Abstract

The structural characteristics of numerous damaged buildings in the Tohoku region were documented soon after the March 11, 2011 Tohoku-Oki earthquake and tsunami by two reconnaissance teams. The first team, sponsored by the American Society of Civil Engineers, focused on structural condition assessments and determination of the tsunami characteristics including inundation depth and flow velocity at a site. The second team, sponsored by NSF, collected LiDAR topographical and structural deformation data for select areas and buildings for improved inundation modeling and structural analysis comparison. Additional estimates of tsunami flow depths and velocities was determined based on analysis of video records and the observed effects on simple benchmark structures in the flow.

Using the collected structural building data and tsunami characteristics, the damage to different buildings was simulated with load estimates based on equations for the various types of fluid loading, including: lateral and buoyant hydrostatic forces; hydrodynamic drag forces from a tsunami surge, and; hydrodynamic bore forces where these occurred. The simulated structural damage was compared with the observed damage, and appropriate assumptions determined for the optimal calibration. These findings are relevant for providing validation and calibration of loading and performance criteria proposed for the new chapter on Tsunami Loads and Effects being developed for the ASCE 7 Standard.

Introduction

The Great East Japan Earthquake (also known as the Tohoku-Oki Earthquake, i.e., the “Offshore Tohoku” Earthquake) and Tohoku Tsunami inflicted substantial damage to many coastal communities in Japan. There is great U.S. interest in studying the effects of the Tohoku Tsunami, due to the analogous threat posed by the Cascadia subduction zone to the Pacific Northwest of North America. (Satake and Atwater, 2007; Geist, 2005; Chock and Robertson, 2011b).

In April, 2011, the American Society of Civil Engineers (ASCE), sponsored a team of engineers to survey tsunami effects on structures along the Tohoku coastline of Honshu (Chock, et al, 2012). The survey objectives were to investigate structural failures and successes and capture additional information for making flow depth and velocity estimates. A subsequent survey funded by NSF RAPID grants captured detailed Light Detection and Ranging (LiDAR) data of selected structures (Olsen, et al, 2012). The 3D data provides a virtual world that enables many types of analyses, including deformation maps of partial concrete wall blow-outs, displacements of damaged steel frame structures, bridge collapses, and other failures. LiDAR scanning is a line of sight technology that emits laser pulses at defined, horizontal and vertical angular increments to produce a 3D point cloud, containing XYZ coordinates for objects that return a portion of the light. Details of typical terrestrial LiDAR acquisition and processing can be found in Kayen et al. (2006) and Olsen et al. (2010, 2012, and *Spectra Chile Maule Earthquake 2010 Special Issue* in publication). The LiDAR survey was performed in June and July 2011, and was assisted by researchers from the Building Research Institute (BRI), National Institute of Land and Infrastructure Management (NILIM) and Saitama University.

The structural building data collected is valuable information to validate numerical models and theories, enabling the quantification and understanding of tsunami forces, failure modes, and for validating non-linear structural response analysis, through a series of case studies. More details of the analysis will be published by Chock et al. 2013. The analysis is based on the methods proposed for a future ASCE 7 Chapter on Tsunami Loads and Effects (Chock et al., 2011a).

Calculated Tsunami Loading

Tsunami loading observed on buildings represented a number of different loading conditions. Some structures were completely surrounded by water and had minimal unbalanced hydrostatic forces, but were subject to hydrodynamic forces. The hydrodynamic drag force, F_d , is described by Equation 1, applied as a uniform load over the depth of the flow:

$$F_d = \frac{1}{2} C_d \rho_s b h v^2 \quad (1)$$

Where: C_d is a drag coefficient based on the shape and size of the structure (FEMA, 2011):

ρ_s is the density of salt water with 7% suspended sediment (taken as 1128 kg/m³)

v is the surge velocity

b is the width of the solid structure perpendicular to the direction of flow, and

h is the depth of flow at the structure

Other structures were subject to differential hydrostatic pressures along with hydrodynamic forces, at least for a portion of their loading history. A hydrostatic uplift force could also be present. For these structures the force is described by Equation 2. The hydrostatic components are applied as triangular pressure distributions increasing with depth while the drag component is applied as uniform pressure:

$$F_h = \frac{1}{2} \rho_s g b (h_1^2 - h_2^2) + \frac{1}{2} C_d \rho_s b h v^2 \quad (2)$$

Where: h_1 and h_2 are the water depths on opposite sides of the structure, and
 g is 9.81 m/s²

Structures subject to flow stagnation have a uniform internal pressure, p , per Equation 3 of:

$$p = \frac{1}{2} \rho_s v^2 \quad (3)$$

Other structures were subject to bore impacts, which include components of hydrostatic, hydrodynamic forces and additional forces resulting from the rejection of the water flow. For a tsunami bore of height h_j travelling over standing water of depth h_s and striking a structural wall oriented perpendicular to the flow direction with a width greater than $3h_b$, the pressure distribution can be estimated by the method in Robertson and Paczkowski et al. (2011), where the transient lateral load per unit width of wall shown in Figure 1 is given by Equation 4.

$$F_b = \rho_s \left(\frac{1}{2} g h_b^2 + h_j v_j^2 + g^{1/3} (h_j v_j)^{4/3} \right) \quad (4)$$

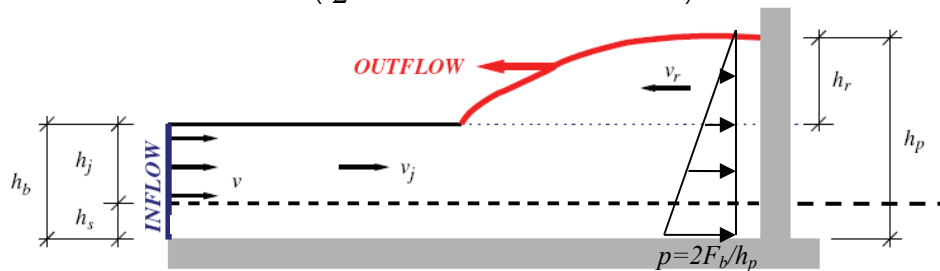


Figure 1. Tsunami bore travelling over standing water and striking a wall

The overall bore force is applied as a triangular pressure distribution with a height of $h_p = h_b + h_r$, where h_r is given by Equation 5:

$$h_r = g^{-\frac{1}{3}} (v_j h_j)^{\frac{2}{3}} \quad (5)$$

In the following sections loading of different buildings is calculated using the equations presented above and known tsunami flow depth and velocity, and the resulting response of the building evaluated and compared to the observed damage in the buildings.

Case Studies of Buildings Subjected to Tsunami Loading during the Tohoku Tsunami

Onagawa Two-Story Cold Storage Building Buoyant Uplift. The reinforced concrete building shown in Figure 2 was lifted by hydrostatic buoyancy off its pile foundation, which did not have tensile capacity due to minimal reinforcing steel development. This building was approximately 22m by 8.7m by 12m tall. The total deadweight of the structure was calculated to be 8995 kN based on detailed measurements of the structural framing and foundation. The refrigerated room portion of the ground floor was effectively sealed off, leading to a neutrally buoyant condition as soon as the water inundation depth reached 7m. The building was lifted off its original site and carried over a low wall (at the left of the Figure 2), before being deposited about 15m inland from its original location.

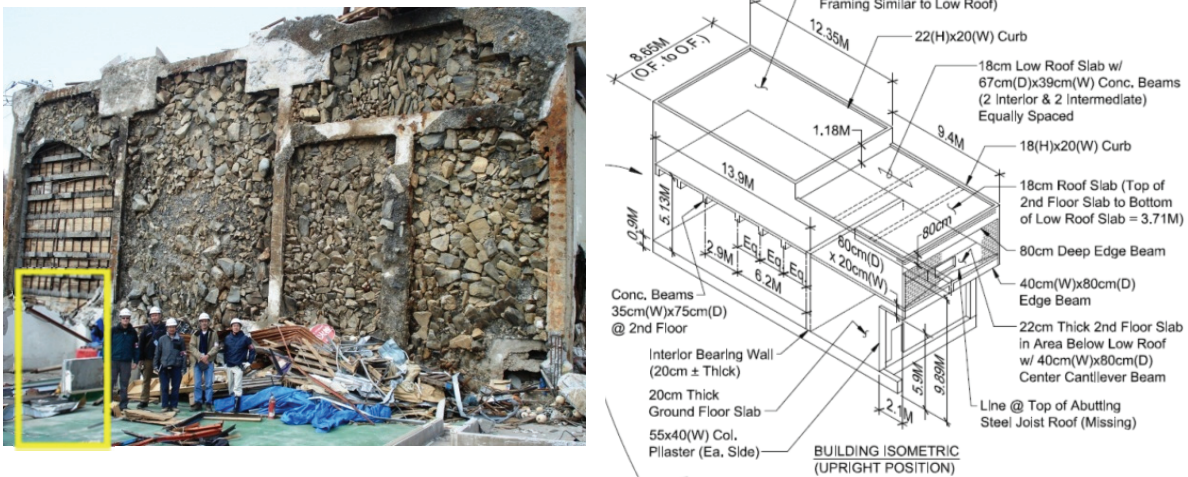


Figure 2. Onagawa uplifted and overturned 2-story RC building – floated over low wall in box

Onagawa Three-Story Steel Building Lateral Pushover. The Onagawa three-story steel moment-resisting frame (Figure 3) was submerged in the flow returning to the ocean estimated from video analysis at about 7.5 m/s (Koshimura and Hayashi, 2012). The building was partly shielded from the inflow by larger concrete buildings. The columns of this frame were wide flange sections with welded 12 mm cover plates to make a box section. The wide flanges were oriented such that they were bent about their weak axis and had pinned base plate detailing. Beams were the “small width” series of JIS 3192 H-shapes with depths of 25cm - 35 cm. Yield and tensile strength are assumed to be consistent with commercial practice of Grade 365MPa and 490 MPa, respectively (similar to U.S. Grade 50).

The flow was sufficient to yield the top and bottom of the second story columns and top of the first story columns assuming 60% blockage of the original enclosure, either from cladding still intact or debris accumulation. At first yield, the calculated lateral drift at the third floor would be about 30 cm with additional flow causing increased displacements. The LiDAR scan of the frame shows a third floor drift of up to 50 cm. It is proposed that once yielding of the structure had occurred with 60% effective cladding blockage, the load was sustained for some period until loss of all remaining cladding later relieved the structure of this lateral pressure. Without such load shedding, collapse would have occurred.



Figure 3 Onagawa 3-story steel frame pushover during drawdown phase

Kesennuma Port Two-Story Warehouse-Office Lateral Pushover. A two-story fish product warehouse in Kesennuma Port was located in between two larger and taller multi-story reinforced concrete buildings. When a seawall was overtopped by the tsunami surge, the flow was directed against the longitudinal face of the building, which was oriented perpendicular to the flow. This was a repetitively framed structure with two-story steel rigid frames in the transverse direction every 6.1m for nine bays (Figure 4). The flow velocity determined from video analysis was 5.5 m/s, and the building was sheared off its foundation when the flow depth reached 5.6m.

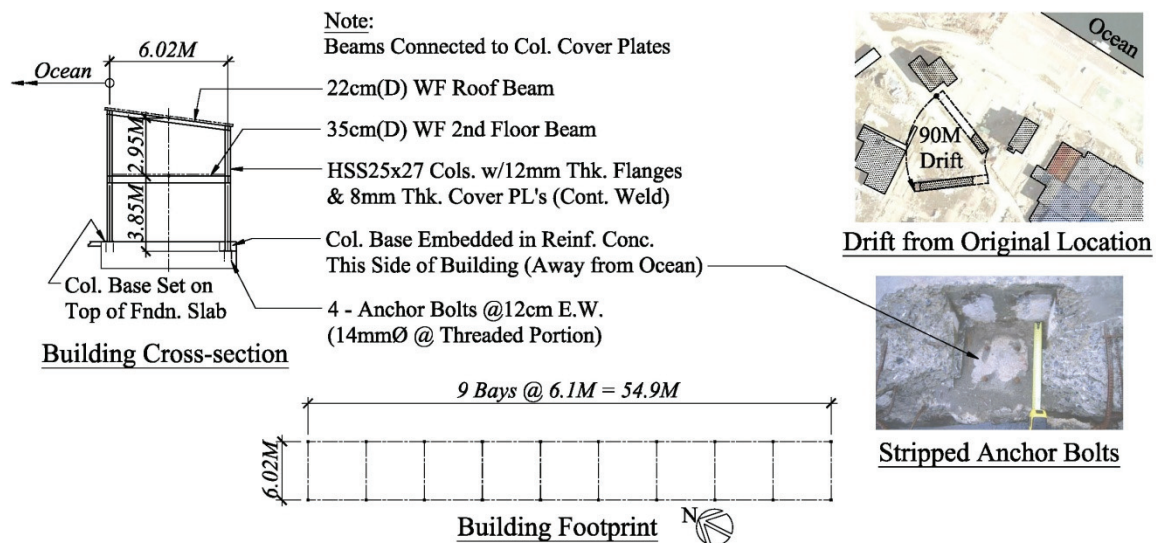


Figure 4. Lateral translation of entire warehouse building and failure of anchor bolts.

The front column base plates were set on the slab-on-grade and the rear base plates were embedded in a 25 cm deep blockout filled with concrete set inboard of a 30 cm-thick reinforced perimeter. Four anchor bolts were provided at the base of each column. Failure occurred by shearing of the 14 mm diameter mild steel anchor bolts (nominal tensile strength of 400 MPa) at the front columns and shear friction breakout of the monolithic concrete edge that was reinforced with 2-15 mm bars assumed to be JIS G3112 SD345 and by bolt shearing at the rear columns. Examination of the debris showed that the first story utilized horizontal steel girts, and the second story was ordinary vertical steel stud framing. This caused the lower story to capture and retain more debris and remain less open. Despite being translated 90m, building contents were still found in the lower floor between the girts on both faces of the lower floor. The upper story was stripped clean of its contents. Analysis of the video with verification by structural analysis using Equation 1 (with a C_d of 2.0) indicates that approximately 75% blockage of the first story cladding and at least 50% of the second story cladding remained prior to failure (Figure 4).

Flow Stagnation Pressurization Analysis of a Concrete Warehouse in Onagawa. This case study was used to verify hydrodynamic pressures during the drawdown phase of the tsunami at Onagawa. Analysis of video taken by a survivor from the top of a reinforced concrete building provided a flow velocity of 7.5 m/s in the free field during drawdown (Koshimura, 2012). The concrete warehouse building (Figure 5) became internally pressurized by flow stagnation during tsunami drawdown. The building only had wall openings facing the drawdown flow and was solid on all other sides. The larger wall panels were observed to have completely failed, with outward highly inelastic deformations showing the formation of membrane action. The smaller wall panels did not fail. It is likely that the walls were subject to several cycles of reversing external and internal pressure forces. However, given that the side walls perpendicular to the shoreline suffered similar damage to the front wall parallel to the shoreline, internal stagnation pressure during drawdown is likely to have been the governing condition.

The wall panels were 120mm thick with a single central layer of 8mm smooth reinforcing spaced at 200mm on center horizontally and vertically. The expected concrete strength was estimated at 30 MPa for nominal 20 MPa concrete based on the vintage of the building. The reinforcing yield and ultimate expected strengths were estimated at 558 MPa and 620 MPa, respectively, assuming Japanese Industrial Standard (JIS) SD490 reinforcing. A finite element analysis was performed, using SAP2000 v15 with non-linear layered shell elements, on the larger and smaller of the typical wall panels. Each layered shell element includes five layers. One layer represents the full thickness of concrete and the other four layers



Figure 5. Concrete wall failure due to internal pressurization (left) and building location (right)

represent wall steel reinforcing at each wall face in each direction. In these walls there was on a single layer of centrally placed steel in each direction. The analysis was compared to deformations measured using a LiDAR scan with a magnitude of around 0.5 m in the larger wall panels, while the smaller panels had negligible lateral deformations. Analysis based on a stagnated hydrodynamic load showed that the larger exterior wall panels failed after flexural yielding of the panels followed by formation of a catenary membrane, followed by shear failure around the perimeter of the wall. The maximum force is plotted against the maximum displacement at the middle of the wall in Figure 6, with the point at the formation of the different limit states shown. Due to the reduced spans, it was calculated that only the edges of the smaller wall panels reached their yield point, therefore some flexural cracking may be expected and was observed in the field, but significant yielding was not expected nor observed. In summary, application of theoretical loading based on internal stagnation pressure and corresponding analysis was able to well characterize the response of the building.

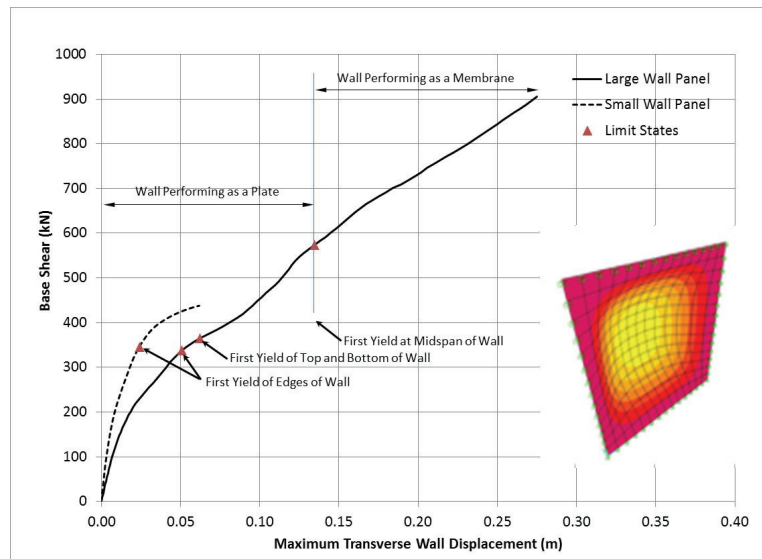


Figure 6. Total applied force versus maximum displacement of the wall and corresponding limit states for large and small wall panels.

Rikuzentakata Tourist Center Concrete Wall Failure due to Combined Hydrostatic &

Hydrodynamic Loading. The Takada Matsubara building in Rikuzentakata, shown in Figure 7, endured a 10.5m tsunami inundation depth with flow of about 7.5 m/s, estimated using analysis of simple “flow surrogate” structures. The tsunami caused failure of its principal transverse shear wall due to unbalanced hydrostatic and hydrodynamic forces of the incoming tsunami surge. The wall was at the rear face of a three-sided concrete box with the opening in the fourth side being a main entrance into the building at the front (north elevation). The tsunami loading was estimated as a triangular distribution of hydrostatic pressure and a uniform distribution pressure representing the hydrodynamic effects.

The wall was analyzed using finite element analysis. The wall panel including the horizontal mid-height beam was modeled utilizing non-linear layered shell elements. Reinforcing steel was sampled and tested and the four reinforcing steel specimens result in a 510 MPa average yield strength, as per JIS G3112 SD 490. The ultimate strength ranges from 647 MPa up to 734 MPa. A multi-step nonlinear time-history analysis was performed to simulate tsunami flow level increased from zero to full inundation depth. In addition to dead load, included for determining P-Delta effects, seven tsunami load stages corresponding to increasing flows depths up to the maximum flow depth of 9.4m were defined. The analysis was terminated at 9.4 m, close to but shy of the 10.5m maximum observed flow depth, when the model became unstable due to excessive deformations and minimal residual strength indicating complete collapse.

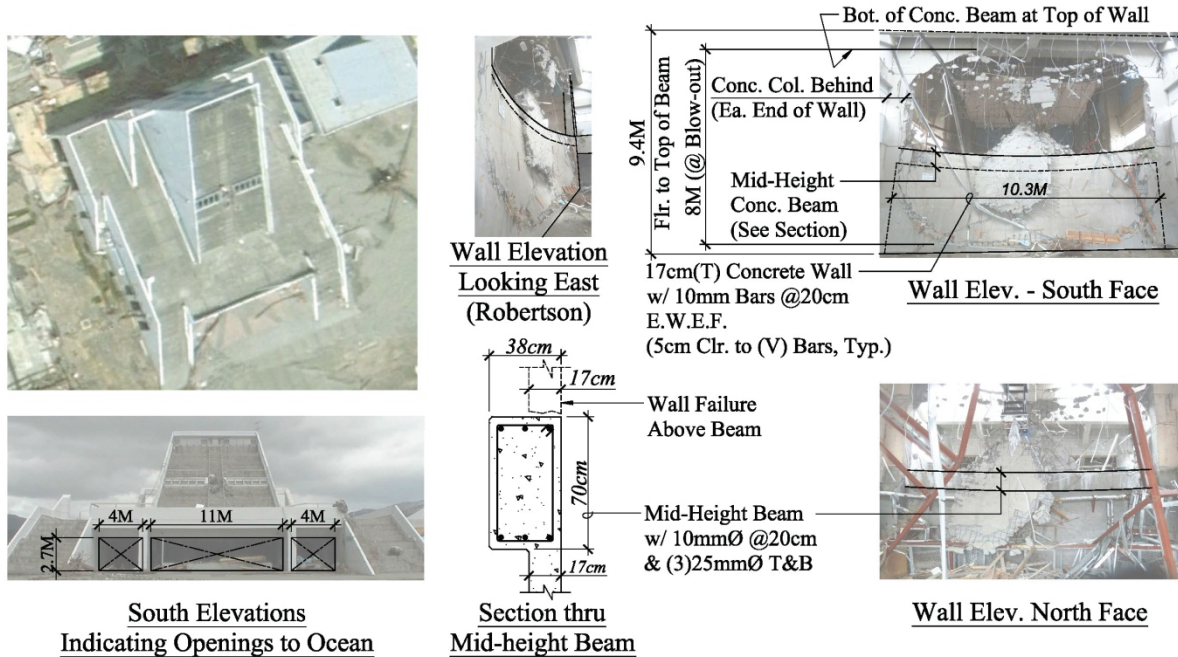


Figure 7. Large wall failure in the Takada Matsubara building in Rikuzentakata

The calculated maximum out-of-plane wall displacement near the center of the wall is plotted against the total lateral load, which equals the integrated tsunami water pressure (Figure 8). The deformed shape of the wall at this stage is also shown. The wall stiffness started to reduce after concrete cracking at the wall base as soon as the tsunami inundation reached 1.6m, and then the slope further reduced as the tsunami water level rose. At the depth of 4.7m, the reinforcing steel yielded at almost all critical areas and the wall changed from a flexural system to a catenary system.

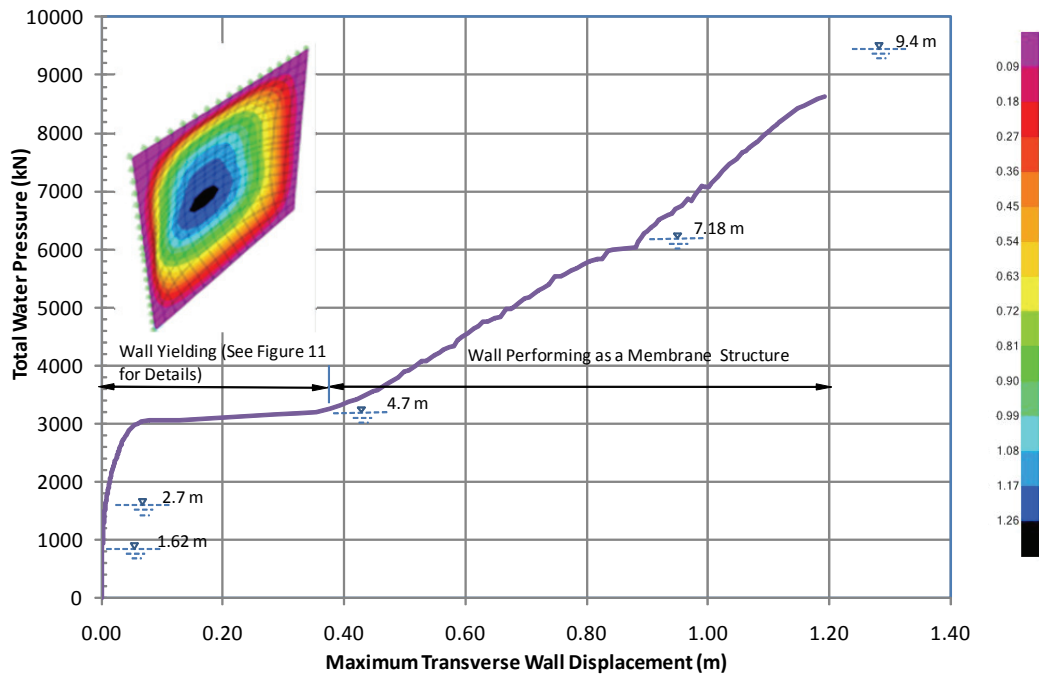


Figure 8. Load history of the total applied force versus maximum displacement of the wall

When the flow level approached 9.4m, reinforcing steel stress reached 730MPa at the wall base and both ends of the horizontal beam. Reinforcing steel stress reached about 650MPa at other areas. The wall is calculated to fail or blow out due to reinforcing steel fracture or loss of bond in the fragmented pieces of the concrete membrane before the tsunami flow level reached the full depth of 10.5m. The calculated displacement at the center of the wall was over 1m.

It is unlikely that wall reinforcing steel was fully developed for the ultimate strength at the supports of the wall. Anchorage and bond failure likely occurred before the reinforcing steel reached its ultimate strength. This final failure mode was not captured in this model; however, except this anchorage failure the failure modes captured in this analysis were consistent with the final condition observed during the survey. It is concluded that the calculated water pressure distribution accurately reproduced the failure modes found in the wall.

Minami Gamou Wastewater Treatment Plant Direct Tsunami Bore Impact on Wall. The Minami Gamou Wastewater Treatment plant has a number of buildings and structures located on the Sendai coastline, south of the main port and approximately 350m from the coastline. Video of this facility in Sendai showed a soliton bore directly striking the longitudinal walls of buildings. Figure 9 shows the ocean facing wall of one particular building with a two story high-bay on one side of the building that failed through out-of-plane flexure. The other side of the building, where the exposed exterior wall was laterally braced by a floor near the mid-height, did not fail. Therefore the upper and lower bound of bore forces can be obtained by studying this building.



Figure 9. Ocean-facing reinforced concrete wall at the Minami Gamou Wastewater Treatment Plant pump station building damaged by direct strike from tsunami bore (a) exterior view, (b) interior view

Using inundation height estimates by the Joint Survey Group and video footage from the roof of the nearby administrative building, bore velocity and height were estimated. Equation 4 provided the wall force due to a bore strike applied with a triangular pressure distribution with maximum pressure of $2F/(h_b+h_r)$ at the base and zero pressure at a height of (h_b+h_r) . For this building the stillwater height, d_s , was estimated to be 0.5 m from the small inflow preceding the bore. The bore height h_b was estimated at 6 m from the video footage. The bore velocity was estimated from the video at 6.5 m/s. Therefore from Equation 5 the rejected water height, h_r , was estimated to be 5.1 m, which was consistent with what was observed at other buildings shown in the video. The resulting pressure distribution and wall cross section represents a maximum applied load of 780 kN/m of width of the wall. The tsunami surge hydrodynamic drag force following the bore impact was estimated at around 50% of the bore impact force.

We compared this force with the tsunami wave pressures given in the Technical Standards of the Overseas Coastal Area Development Institute of Japan (OCADI, 2009) and that of the Structural Design Method of Buildings for Tsunami Resistance (Okada, et al, 2005). The technical standards of the Overseas Coastal Area Development Institute of Japan utilize a maximum pressure equivalent to 2.2 times the hydrostatic pressure for the incident tsunami height above the stillwater level applied over a triangular distribution up to 3 times the incident tsunami bore height, and the maximum pressure applied uniformly over the stillwater depth below the bore. Another distribution used in Japanese design guidelines is an equivalent hydrostatic pressure acting over 3 times the tsunami depth, based on the “SMBTR” method of the Building Technology Research Institute.

Structural drawings for the damaged buildings were obtained from the plant management, which enabled a finite element model of the building to be developed for the area of the wall failure. The wall, column, beam and roof slab properties were modeled in accordance with the structural drawings.

A comparison of the deformation pattern in the wall from a LiDAR scan and the corresponding finite element analysis is shown in Figure 10. With the assumed material properties, the magnitudes of the highly inelastic wall displacements were similar to the observed permanent deformation from the LiDAR imaging. The distribution and magnitude of the highly inelastic calculated wall displacements were in agreement. The bore forces were found to be sufficient to create mid-height and bottom flexural yielding in the wall and columns, and yielding of the roof beams and slab at the top of wall, consistent with the failure mode observed.

Once all the critical components of the wall had yielded, there was minimal post-yield stiffness as the effects of material hardening and large displacement stiffening were offset by the distribution of yielding and P-delta effects. It was concluded that the calculated pressure distribution accurately captured the failure mode of the wall, with the theoretical bore pressure distribution most accurate. The OCADI procedure calculated similar deformation magnitude and profile, while the SMBTR method significantly overestimated the deformations. Applying the different loading distributions to the other side of the building with the wall braced near the mid-height, resulted in minimal calculated damage, consistent with the observed behavior of the building.

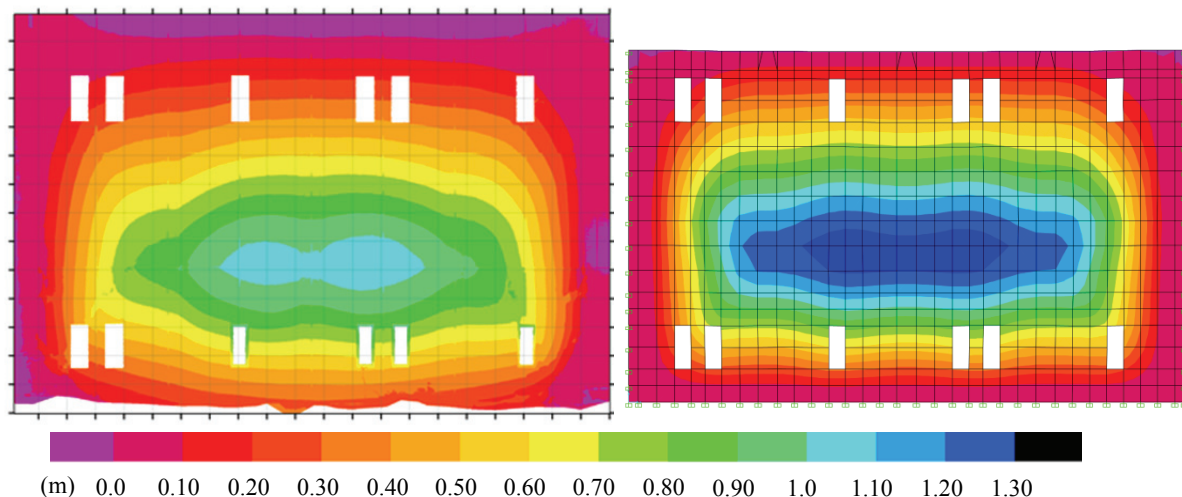


Figure 10. Deformation modeling using a triangulated LIDAR scan showing out-of-plane deformation (left) compared to a FEM analysis of damaged wall (right).

Conclusions

Great earthquakes and tsunamis subject structures to the largest transient and sustained forces that they would ever experience. For critical facilities that may necessarily exist within coastal zone subject to tsunami hazard, an adequate set of design provisions should be capable of addressing all hydrostatic and hydrodynamic forces generated by tsunami flow conditions. The preceding analyses from the Tohoku Tsunami demonstrate that there are sufficiently reliable tools for structural load characterization and analysis of suitably defined tsunami flow conditions. The measurements (both LiDAR and directly taken) from these case studies validate the equations when capturing nonlinear behavior in the numerical modeling.

References

- Chock, G., Carden, L. Robertson I., Olsen M., Yu, G., 2013. "Tohoku Tsunami-Induced Building Failure Analysis with Implications for U.S. Tsunami and Seismic Design Codes", *Earthquake Spectra – Tokoku, Japan Earthquake Special Issue, accepted, in publication.*
- Chock, G., Robertson, I., Kriebel, D., Francis, M., and Nistor, I., 2012. "Tohoku Japan Tsunami of March 11, 2011 – Performance of Structures", *ASCE/SEI Report, in Publication.*
- Chock, G., Robertson, I.N., Riggs, H.R., 2011a. "Tsunami Structural Design Provisions for a New Update of Building Codes and Performance-Based Engineering", in *Proceedings, Solutions to Coastal Disasters 2011*, ASCE.
- Chock, G., Robertson, I., 2011b. "The Tohoku, Japan, Tsunami of March 11, 2011: Effects on Structures", *EERI Special Earthquake Report, Earthquake Engineering Research Institute, Oakland, California.*
- Geist, E., 2005. "Local Tsunami Hazards in the Pacific Northwest from Cascadia Subduction Zone Earthquakes", *U.S. Geological Survey Professional Paper #1661-B.*
- Kayen, R., Pack, R., Bay, J., Sugimoto, S., and Tanaka H. 2006, "Terrestrial-LiDAR visualization of surface and structural deformations of the 2004 Nigata Ken Chuetsu Japan Earthquake", *Earthquake Spectra*, **22**(S1), S147-S162.
- Koshimura, S. and Hayashi, S. 2012. "Interpretation of Tsunami Flow Characteristics by Video Analysis", in *Proceedings, 9th International Conference on Urban Earthquake Engineering/ 4th Asia Conference on Earthquake Engineering*, Tokyo Institute of Technology, Tokyo.
- Okada, T, Sugano, T., Ishikawa, T., Ohgi, T., Takai, S., and Hamabe, C., 2005. "Structural Design Method of Buildings for Tsunami Resistance (Proposed)", *The Building Letter*, Nov., 2004, The Building Center of Japan - Building Technology Research Institute.
- Olsen, M.J., Kuester, F., Chang, B., and Hutchinson, T., 2010. "Terrestrial laser scanning based structural damage assessment", *Journal of Computing in Civil Engineering*, **24**(3), p. 264-272.
- Olsen, M.J., Carden, L.P., Silvia, E.P., Chock, G., Robertson, I.N., and Yim, S. 2012. "Capturing the Impacts: 3D Scanning after the 2011 Tohoku Earthquake and Tsunami", in *Proceedings, 9th International Conference on Urban Earthquake Engineering/ 4th Asia Conference on Earthquake Engineering*, Tokyo Institute of Technology, Tokyo, Japan.
- Olsen M.J., Cheung, K.F., Yamazaki, Y., Butcher, S.M., Garlock, M., Yim, S.C., Piaskowy, S., Robertson, I., Burgos L., and Young Y.L., 2012. "Damage Assessment of the 2010 Chile Earthquake and Tsunami using ground-based LiDAR", *Earthquake Spectra* (in publication).
- Overseas Coastal Area Development Institute (OCADI) of Japan, 2009. "Tsunamis", *Technical Standards and Commentaries for Ports and Harbour Facilities in Japan*, Chapter 2 Part 5.
- Robertson I.N., Paczkowski, K., Riggs, H.R., Mohamed, A. 2011. "Tsunami Bore Forces on Walls", in *Proceedings, ASME 2011 30th International Conference on Ocean, Offshore and Arctic Engineering*, Rotterdam, The Netherlands.
- Satake, K., and Atwater, B., 2007. "Long-term Perspectives on Giant Earthquakes and Tsunamis at Subduction Zones", *Annual Review of Earth and Planetary Sciences*, **35**, pp. 349-374.